

Central Lancashire Online Knowledge (CLoK)

Title	Dynamic visualisation and measurement of cartilage morphology by magnetic resonance imaging-based knee kinematics
Type	Article
URL	https://clock.uclan.ac.uk/48166/
DOI	https://doi.org/10.1504/ijcat.2023.132403
Date	2023
Citation	Quan, Wei, Wang, Zhe and Shark, Lik (2023) Dynamic visualisation and measurement of cartilage morphology by magnetic resonance imaging-based knee kinematics. <i>International Journal of Computer Applications in Technology</i> , 71 (4). pp. 321-331. ISSN 0952-8091
Creators	Quan, Wei, Wang, Zhe and Shark, Lik

It is advisable to refer to the publisher's version if you intend to cite from the work.
<https://doi.org/10.1504/ijcat.2023.132403>

For information about Research at UCLan please go to <http://www.uclan.ac.uk/research/>

All outputs in CLoK are protected by Intellectual Property Rights law, including Copyright law. Copyright, IPR and Moral Rights for the works on this site are retained by the individual authors and/or other copyright owners. Terms and conditions for use of this material are defined in the <http://clock.uclan.ac.uk/policies/>

Dynamic visualisation and measurement of cartilage morphology by magnetic resonance imaging-based knee kinematics

Wei Quan*, Zhe Wang and Lik-Kwan Shark

Applied Digital Signal and Image Processing (ADSIP) Research Centre,
University of Central Lancashire,
Preston, England, UK
Email: WQuan@uclan.ac.uk
Email: ZWang28@uclan.ac.uk
Email: LShark@uclan.ac.uk
*Corresponding author

Abstract: To address the limitation in static imaging for clinical diagnosis of knee joints based on a snapshot of the knee in a fix pose, an approach is presented for quantitative assessment of knee joints in a dynamic manner. The core of the proposed approach is based on kinematics of the knee bones, whereby articulation of knee joints derived from magnetic resonance imaging is emulated by capturing and mimicking the movement of an artificial anatomical knee model. Through bone-based kinematic emulation, dynamic visualisation and measurement of cartilage morphology are demonstrated by focusing on tibiofemoral cartilage thickness as a function of knee joint movement angle. In particular, the differences in dynamic tibiofemoral cartilage thickness between two knees with mild and severe osteoarthritis are illustrated to show the effectiveness and potential of the proposed approach. Also presented is an interactive visualisation and measurement tool based on Matlab for dynamic knee joint assessment.

Keywords: kinematics; magnetic resonance imaging; knee assessment; motion tracking; modelling and emulation; knee joint landmark; cartilage thickness.

Reference to this paper should be made as follows: Quan, W., Wang, Z. and Shark, L-K. (xxxx) 'Dynamic visualisation and measurement of cartilage morphology by magnetic resonance imaging-based knee kinematics', *Int. J. Computer Applications in Technology*, Vol. XX, No. X, pp.xxx-xxx.

Biographical notes: Wei Quan is a Senior Lecturer at the University of Central Lancashire in the UK. His research interests include signal and image processing, visual information processing, biomedical engineering, computer vision and machine learning. He is a Member of the Applied Digital Signal and Image Processing (ADSIP) Research Centre.

Zhe Wang obtained his MSc by Research degree from the University of Central Lancashire, UK in 2022. He was working on a research project for developing an immersive platform for the assessment of knee osteoarthritis.

Lik-Kwan Shark is a fellow of IET and the Chair Professor of Signal and Image Processing at the University of Central Lancashire in the UK. He founded and heads two centres which are the Applied Digital Signal and Image Processing (ADSIP) Research Centre and the Advanced Digital Manufacturing Technology (ADMT) Research Centre.

This paper is a revised and expanded version of paper entitled 'Development of Bone-based Kinematics from Magnetic Resonance Imaging for Immersive Assessment of Knee Joints' presented at the '5th International Conference on Image and Graphics Processing (ICIGP 2022)', Beijing, 7-9 January 2022.

1 Introduction

In the knee where three bones of femur, tibia and patella articulate with each other, articular cartilage covers their bony articulating surfaces and provides necessary viscoelastic tissues to enable smooth joint movement (Gahunia et al., 2020). During daily activities, the knee is repeatedly exposed to heavy loads and stress, which often

reach several times body weight (D'Lima et al., 2012), leading to gradual wear and eventual degeneration of articular cartilage, with the incidence of knee Osteoarthritis (OA) increasing with age (Wick et al., 2014). As a result of the demographic trends in ageing, there is an increasing demand for not only diagnostic imaging of the knee, but also quantitative clinical tools for its assessment and health monitoring.

There are several imaging modalities available for assessment of knee OA (Spain et al., 2015). Owing the wide availability and cost-effectiveness, the conventional approach based on radiographic images is still most common in routine clinical practice, with diagnosis of knee OA mainly based on bony tissues (NICE, 2014). By providing 3D anatomical details without the need of ionising radiation, Magnetic Resonance Imaging (MRI) is increasingly used for quantitative evaluation of knee OA (Sowers et al., 2003), particularly, cartilage morphology in terms of thickness, volume and surface area (Eckstein et al., 2006).

However, there is an inherent limitation in static imaging of dynamic joints for quantitative evaluation of knee OA, because it is based on a ‘snapshot’ of the knee in a fixed pose. This has led to the development presented in this paper to emulate articulation of knee joints derived from MRI, thereby enabling dynamic visualisation and measurement of cartilage morphology based on joint movement angle.

For anatomy-based emulation of knee joint articulation, there exist three approaches based on static, kinematic and musculoskeletal models, respectively. By using a small number of Computerised Tomography (CT) or MRI images of a knee joint captured at specific flexion angles, the static model approach constructs a 3D anatomical model of each knee bone at each flexion angle to obtain the poses of knee bones (Song et al., 2015). It does not require joint motion capture and can be extended to cover more comprehensive flexion angles of knee articulation by taking additional CT or MRI images from patients (Tischer et al., 2016).

In comparison with the static model approach, the kinematic model approach can emulate the poses of knee bones over more flexion angles, with the help of kinematics (Hamai et al., 2013). The approach consists of two processing stages, namely, model calibration and knee motion generation. With a high-resolution anatomical model of the knee joint constructed in the model calibration stage, knee joint motion is captured through a range of flexion angles using MRI images and fluoroscopic videos (Kedgley et al., 2015). Through image registration methods, such as simulating annealing and Powell’s direction set methods (Chen et al., 2013), the joint kinematic data, including joint positions and angles, are obtained and applied to drive the knee motion using forward kinematics in the knee motion generation stage.

The musculoskeletal model approach can be considered as an extension of the kinematic model with the muscles and ligaments attached to the joints. It has been primarily used in the research involving the study of muscles reaction in knee motion, which contains similar processing stages as that in the kinematic model (Kainz et al., 2016). Through Hill-type like models that describe a single muscle fibre and relate the force on muscle and change of muscle length, a non-linear equation is applied to simulate the muscle interaction. Since it is difficult to obtain a sequence of muscle activation values over time to drive the model, Lloyd and Besier (2003) proposed a solution to use electromyography (EMG) signals recorded in the biomechanical experiment. Musculoskeletal model is more complex than kinematic and static models because of forces modelling.

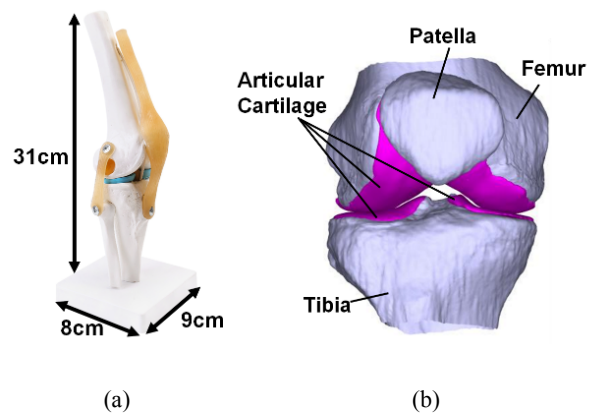
Presented in this paper is a new kinematic model approach that is practically more feasible without requiring multiple MRI images and fluoroscopic videos, whereby articulation of knee joints derived from MRI is achieved by capturing and mimicking the movement of an artificial anatomical model of a knee joint based on the relative position and orientation of the three knee bones (Wang et al., 2022). By using the proposed bone-based kinematic model, the paper also presents dynamic visualisation and measurement of cartilage morphology with a particular focus on tibiofemoral cartilage thickness, thereby demonstrating the clinical potential for qualitative and quantitative diagnosis of knee joints in a more comprehensive and intuitive manner without prolonging assessment time.

The rest of the paper is organised as follows. The first part on bone-based kinematic model consists of three sections with Section 2 introducing the anatomical knee models, Section 3 covering anatomical landmark detection and Section 4 describing each processing stage of kinematic emulation for knee joint articulation in detail. The second part on dynamic cartilage morphology consists of two sections with Section 5 presenting measurement of dynamic tibiofemoral cartilage thickness and Section 6 demonstrating the results based on two different knee joints diagnosed to have mild and severe OA. Finally, the concluding remarks are given in Section 7.

2 Knee models

Two types of knee models had been used in this work, which are an Artificial Anatomical Knee Model (AAKM) and patient-specific Anatomical Knee Joint Model (AKJM) as shown in Figure 1. While the former was used for generating the moving trajectory of the knee, the latter was used to emulate articulation of knee joints for subsequent dynamic visualisation and measurement of knee cartilage morphology.

Figure 1 Knee models: (a) AAKM and (b) AKJM



AAKM is an anatomical model of the knee joint that was designed for the anatomy and clinical study. It is a life-size, moveable knee model that was cast from a real adult specimen. It contains the bone structures of the knee joint

with flexible and artificial ligament, which is able to demonstrate flexion, extension, internal and external rotation and gliding motion.

AKJM is a patient-specific 3D knee model built from MRI images. There exist various MRI acquisition sequences for imaging of different anatomical structures. For this work, a Philips 3D Watsf sequence, with the repetition time between successive excitation pulses (TR) set to 15 ms, the echo time for signal acquisition (TE) set to 5.6 ms, and the magnetisation flip angle set to 25°, was used to produce sagittal fat-saturated MR images of knee joints with 0.36×0.36 mm for pixel size and 0.7 mm for slice thickness (Balamoody et al., 2010).

To construct the anatomical model from MRI for emulation of knee joint articulation, bone and cartilage were segmented by an experienced manual segmenter, using a semi-automated livewire algorithm (Endpoint segmentation software, Imorphics, Manchester, UK). This generates a set of contours, one for each slice of the MR image. The number of contours per slide can be upto a maximum of seven, corresponding to three bone regions, namely, femur, tibia and patella, as well as four tibiofemoral cartilage regions (medial and lateral regions at the end of femur and at the top of tibia) and patella cartilage region. 3D surfaces were then generated from the stack of contours using a marching-cubes algorithm, followed by quadratic smoothing of the resultant surfaces (Shark et al., 2016). For the AKJM model shown in Figure 1(b), the cartilage regions are shown in purple colour.

3 Joint landmark detection

From the perspective of motion, knee joint articulation consists of tibiofemoral articulation with femur rotating against tibia and patellofemoral articulation with patella sliding against femur. A set of anatomical landmarks on the three bony surfaces were identified from AKJM and used to provide a geometrical reference of the relative positions between the three bones for kinematic emulation of knee joint articulation.

As shown in Figure 2, the set of joint landmarks on AKJM consists of FLM1 and FLM2 on femur, PLM1 and PLM2 on patella and TLM1 to TLM3 on tibia. While FLM1 and FLM2 are used to form the epicondylar axis of femur and its posture during the movement, PLM1 and PLM2 are used to locate the position of patella and TLM1 to TLM3 are used for kinematic validation.

With FLM1 and FLM2 defined as the Medial Epicondyle Point (MEP) and Lateral Epicondyle Point (LEP) of the femur, their 3D positions on AKJM were identified manually first based on the femur's bony protrusions, thereby providing a pair of 3D reference coordinates (Shark et al., 2016). Using the epicondylar axis defined by MEP and LEP, AKJM was then transformed into the position with its epicondylar axis aligning with the Z-axis in the Cartesian coordinate system and with LEP at the origin as shown in Figure 3. With the X-axis in the inferior-

superior direction and the Y-axis in the anterior-posterior direction, the extreme coordinates of the femur, patella and tibia bones of AKJM were then searched on the X-, Y- and Z-axes to yield the landmarks of PLM1, PLM2, TLM1, TLM2 and TLM3. The characteristics of all joint landmarks used in this work are described in Table 1.

Figure 2 Joint landmarks on AKJM: (a) medial view of AKJM and (b) lateral view of AKJM

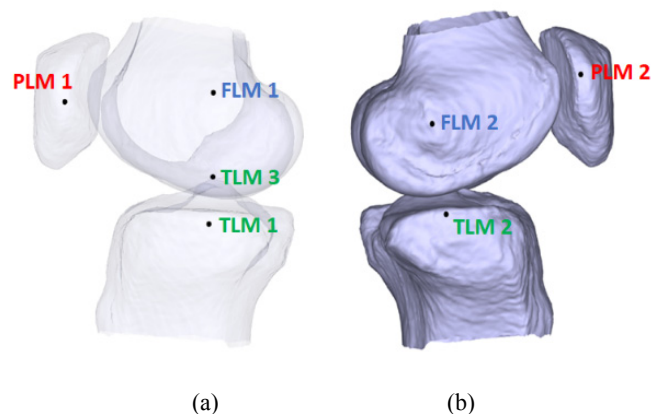


Figure 3 AKJM coordinate system

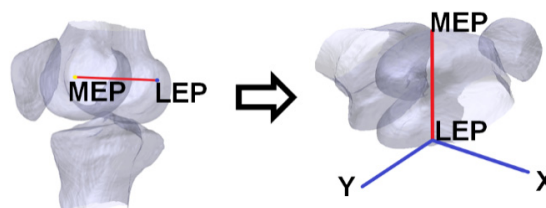
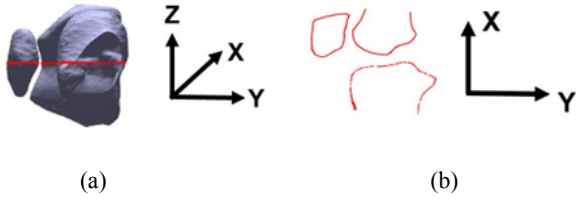


Table 1 AKJM joint landmarks

Landmark	Joint	Location
FLM1	Femur	Medial epicondyle point
FLM2	Femur	Lateral epicondyle point
PLM1	Patella	Largest coordinate value along Z-axis
PLM2	Patella	Smallest coordinate value along Z-axis
TLM1	Tibia	Largest coordinate value along Z-axis
TLM2	Tibia	Smallest coordinate value along Z-axis
TLM3	Tibia	Largest coordinate value along Y-axis

In addition, a central reference plane was created to contain three cross-sections of femur, tibia and patella, for measurements of the relative bone poses in terms of their relative distances for position control in articulation emulation. The central reference plane was defined as the plane perpendicular to the epicondylar axis and passing through the midpoint (denoted as CP) between MEP and LEP along the epicondylar axis. This is illustrated in Figure 4, where the central reference plane, shown as a red line from the top view of AKJM in Figure 4(a), cuts through the femur, tibia and patella to produce three cross-sections shown in Figure 4(b).

Figure 4 Three cross-sections: (a) top view and (b) profile view

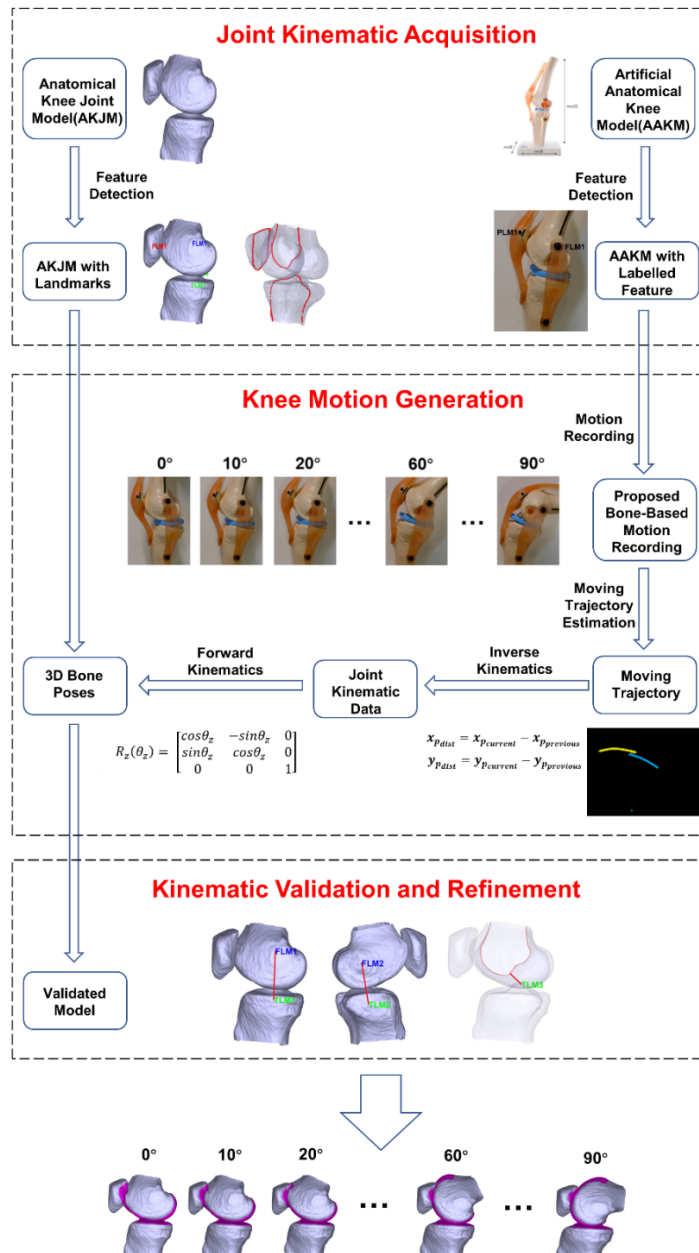


4 Kinematic emulation

The main purpose of kinematic emulation is to generate appropriate motion for knee joint articulation. A modified version of the kinematic model (Hamai et al., 2013) was developed for emulation of knee joint articulation in this work, which consists of three processing stages, namely,

(a) kinematic acquisition, (b) motion generation and (c) kinematic validation. In the kinematic acquisition stage, knee joint articulation was captured through a comprehensive range of flexion angles based on the moving trajectory of AAKM. In the motion generation stage, the joint kinematic data were estimated from the captured motion data through the inverse kinematics (Reinbolt et al., 2005), and then applied to AKJM constructed from MRI images to emulate knee joint articulation based on forward kinematics (Kucuk and Bingul, 2006). Finally, the kinematic validation stage checked the emulated knee joint articulation based on appropriateness of relative poses among the three bones without incorrect intersection and disproportionate gaps, and refined the kinematics accordingly. The flow diagram of the proposed bone-based kinematics is illustrated in Figure 5 and its details are explained in the remaining part of this section.

Figure 5 Flow diagram of proposed kinematic emulation

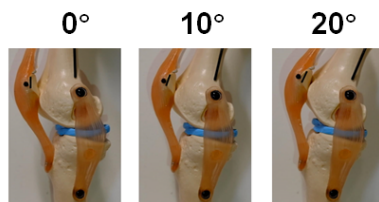


4.1 Kinematic acquisition

Kinematic acquisition aims to compute the joint kinematic data from AAKM's articulation through motion recording and moving trajectory estimation. While motion recording captures video of AAKM's articulation, moving trajectory is estimated by extracting and identifying the motion capture landmarks placed on AAKM.

A Sony A7 III digital camera with a tripod was used to capture the side movement of AAKM. During the recording, the femur of AAKM was manually manipulated and slowly moved from 0 to 90° with respect to the stationary tibia. Figure 6 shows a set of recording samples, where the recorded AAKM images are seen to consist of five black position and orientation markers placed on AAKM, with a small black circle on patella corresponding to PLM1 on AKJM, two large black circles with one on tibia and one on femur corresponding to FLM1 on AKJM, a short black line on patella and a long black line on femur indicating their angular orientations with respect to the stationary tibia.

Figure 6 Samples of AAKM's movement



A sequence of image processing operations was applied to each frame of the video recording of AAKM's movement to

Figure 7 Extraction of position and orientation markers

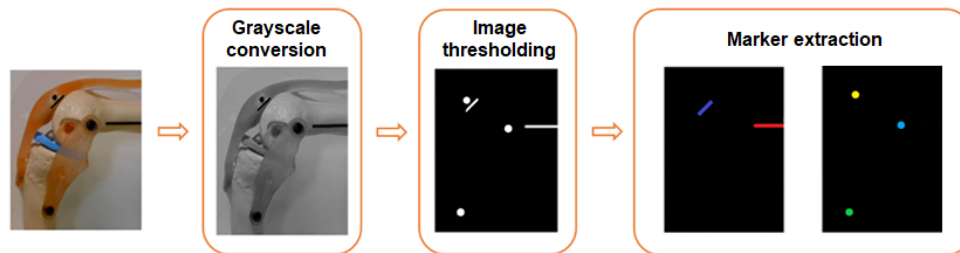
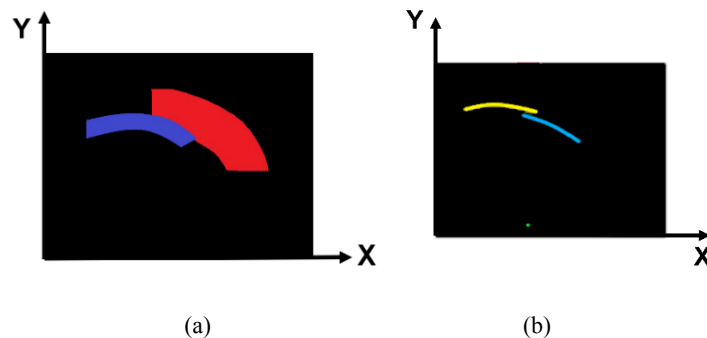


Figure 8 Moving trajectories of AAKM's three bones: (a) orientation and (b) translation



extract the image coordinates of each motion capture marker, which consists of greyscale conversion, image thresholding and marker extraction as illustrated in Figure 7 with example images. From the example greyscale image produced by the greyscale conversion step, it is seen that all parts of AAKM and background are much brighter than the black position and orientation markers and this enables the image thresholding step to be performed on the inverted greyscale image based on a fixed thresholding to produce a binary image containing all the black position and orientation markers on AAKM. For the two line-based orientation markers in the binary image, they are extracted by applying the Hough transform (Wang et al., 2014), with the short straight line used to indicate patella flexion angle (shown in blue) and the long straight line used to indicate femur flexion angle (shown in red) with respect to tibia. For the three circle-based position markers in the binary image, they are extracted based on their locations, with the highest one used to indicate the PLM1 position (shown in yellow), the middle one used to indicate the FLM1 position (shown in blue), and the lowest one used to indicate the tibia position (shown in green).

By moving the femur of AAKM from 0 to 90° with respect to the stationary tibia, Figure 8 shows the trajectories of the position and orientation markers extracted from each frame of the video recording. While the blue and red arcs traced by the line-based orientation markers as shown in Figure 8(a) indicate the angular change of patella and femur, the yellow and blue curve traced by circle-based position markers as shown in Figure 8(b) indicate the position change of patella and femur in terms of PLM1 and FLM1.

By computing the position displacement of circle-based position markers and angular difference of line-based orientation markers based on Figure 8, the kinematic data of femur and patella at each knee flexion angle can be derived by the inverse kinematics (Grochow et al., 2004). Owing the tibia of AAKM being hold stationary during femur movement, the green circle in Figure 8(b) is seen to stay at the same position and no kinematic estimation is required for tibia.

4.2 Motion generation

Having obtained the kinematic data of each bone, the movements of femur and patella were emulated by mimicking the trajectories of the position and orientation markers placed on AAKM. In particular, for each position marker along its respective moving trajectory shown in Figure 8(b), let $x_{p_{current}}$ and $y_{p_{current}}$ denote its current location and let $x_{p_{previous}}$ and $y_{p_{previous}}$ denote its previous location, then the associated bone is translated in each step along the X - and Y -axes by

$$x_{p_{dist}} = x_{p_{current}} - x_{p_{previous}} \quad (1)$$

$$y_{p_{dist}} = y_{p_{current}} - y_{p_{previous}} \quad (2)$$

Similarly, let θ_z denote the rotation of each orientation marker along its respective moving trajectory, then the associated bone is rotated in each step around the Z -axis by applying the rotation matrix of

$$R_z(\theta_z) = \begin{bmatrix} \cos\theta_z & -\sin\theta_z & 0 \\ \sin\theta_z & \cos\theta_z & 0 \\ 0 & 0 & 1 \end{bmatrix}$$

As an example based on the kinematic data estimated from the motion of AAKM, Figure 9 illustrates the individual motion generated for the femur and patella of AKJM from 0 to 90° in step of 30°, where both femur and patella are seen to exhibit larger translation in the X -axis than that in the Y -axis and the femur is seen to be significantly rotated in each step compared with patella as one would expect.

As another example, Figure 10 illustrates whole knee joint articulation based on AKJM from 0 to 90° in step of 10°, where the patella is seen to gradually shift to the right in order to keep in touch with the changing bony contour of the femur as the femur rotates, as one would expect.

Figure 9 Samples of motion generation: (a) femur and (b) patella

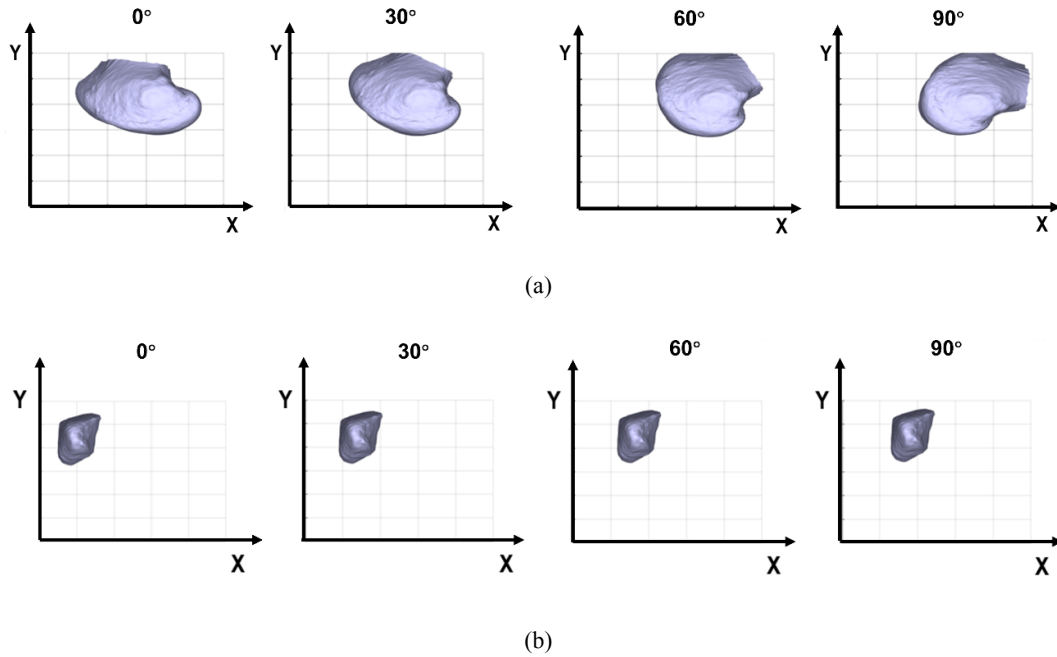
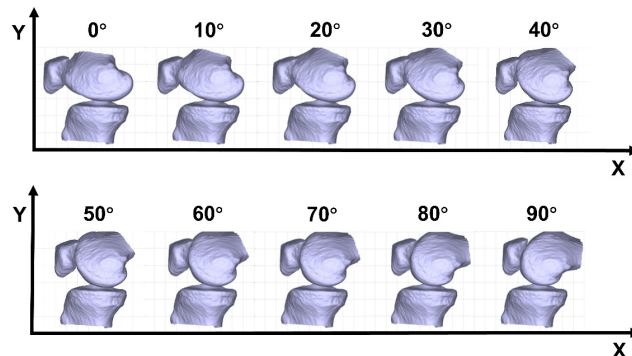


Figure 10 Samples of motion generation for AKJM



4.3 Kinematic validation

Two possible problems could be introduced in the process of knee motion generation, which are bone intersection and excessive gap. While bone intersection indicates the distance between bones is too close to each other during the flexion, excessive gap shows the opposite scenario. Meister et al. (2000) proposed the solutions by using pre-defined ranges of distance measurement between key locations of bones to determine the correctness of knee emulation and adjust the bone distances through the refinement process.

In this work, distance criteria were developed in which the distances measured between three pairs of landmarks are utilised to verify the correctness of the emulation, which are (a) the distance between FLM1 and TLM1; (b) the distance between FLM2 and TLM2 and (c) the shortest distance between TLM3 and the points on the cross-section of the femur, as shown in Figure 11, with their appropriate ranges defined in Table 2. For the cases where measured distances at a particular flexion angle are smaller than the defined ranges, the refinement process moves the femur away from the tibia to reach the minimum value of the defined ranges. For the cases where measured distances are larger than the defined ranges, the refinement moves the femur close to the tibia to reach the maximum value of the defined ranges.

Figure 11 Three measurements of distance for kinematic validation

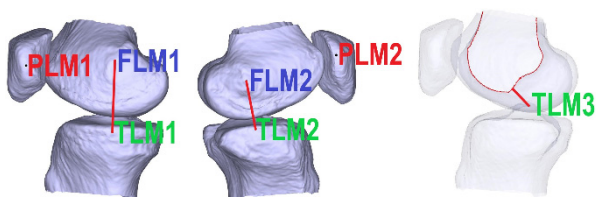


Table 2 Definition of distance measured for kinematic validation

Description	Suitable range
Distance between FLM1 and TLM1	56.9–67.9 mm
Distance between FLM2 and TLM2	59.0–74.0 mm
Distance between TLM3 and cross-sections	9.5–19.2 mm

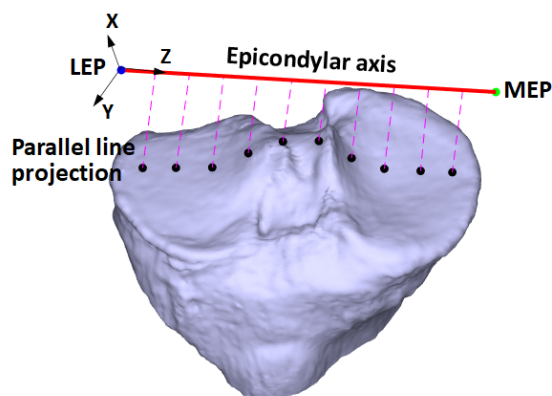
5 Dynamic cartilage morphology

Through kinematic emulation of patient-specific AKJM derived from MRI presented in the previous section, it becomes possible for cartilage morphology to be visualised and measured from all possible viewpoints in a dynamic manner based on knee joint angle. With tibiofemoral joint as the main weight-bearing part of the knee, this section focuses on measurement of its cartilage thickness.

Dynamic tibiofemoral cartilage thickness consists of femoral cartilage thickness and tibial cartilage thickness as a

function of knee joint angle. This was measured through bone-based kinematics by rotating femur with respect to tibia to result in different regions of the femoral cartilage to move onto the top of the tibial plateau. Illustrated in Figure 12 are generation of measurement points across the middle line of the tibial plateau for estimation of dynamic tibiofemoral cartilage thickness. With the number of measurement points depending on the resolution required, 10 measurement points are illustrated in the figure as an example and are obtained based on equal distance interval between LEP and MEP at two ends of the epicondylar axis. By projecting the measurement points downwards onto the tibia (shown as parallel red lines), a corresponding set of surface landmarks for measurement of tibiofemoral cartilage thickness is produced across the middle elevation profile of the tibial plateau (shown by black dots at the end of parallel red lines).

Figure 12 Generation of measurement points



Illustrated in Figure 13 are cartilage thickness estimation of tibia and femur. For the former, it is estimated based on the distance between the tibial surface landmarks and their corresponding points directly above on the tibial cartilage surface along the parallel projection lines, as shown in Figure 13(a). For the latter, it is estimated as the distance between the corresponding inner and outer surface points of the femoral cartilage along the parallel projection lines between the tibial surface landmarks and the epicondylar axis, as shown in Figure 13(b).

Measurement of dynamic tibiofemoral cartilage thickness involves rotation of femur for each knee joint angle before cartilage thickness estimation. While tibial cartilage thickness can be estimated by just one computation because of stationary tibia, multiple computations are required to estimate the femoral cartilage thickness for each rotation angle. Illustrated in Figure 14 are tibiofemoral cartilage thickness estimated at knee flexion angles of 0°, 45° and 90° for 10 measurement points denoted by CM1 to CM10 starting from LEP, where the changes in cartilage thickness values for some measurement points at different joint angles are seen to be significant.

Figure 13 Cartilage thickness estimation: (a) tibial and (b) femoral

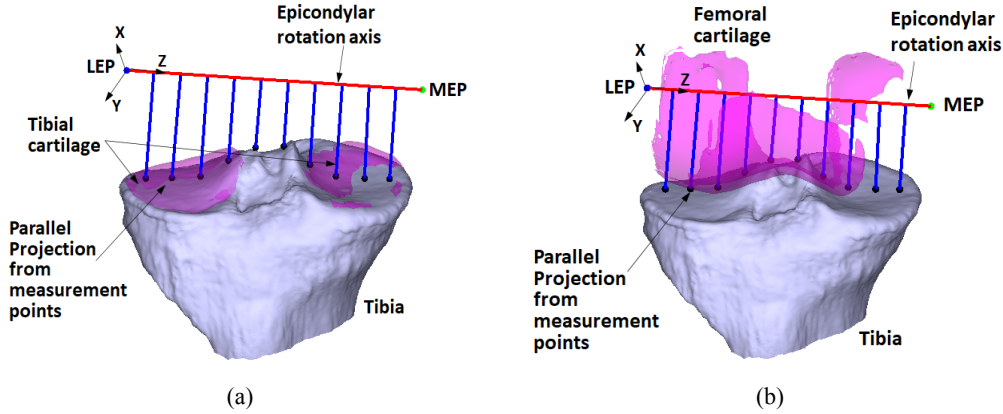
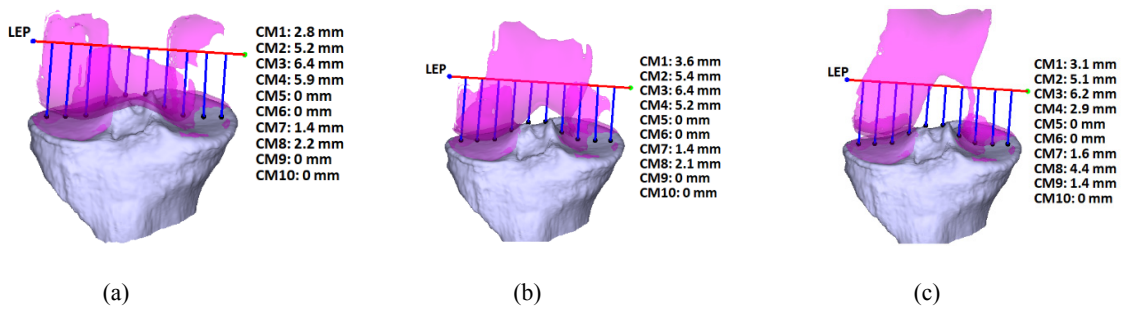


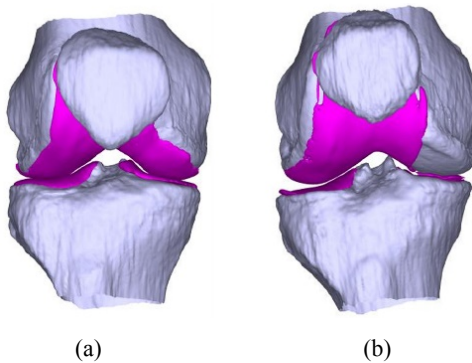
Figure 14 Examples of angle-based tibiofemoral cartilage thickness: (a) 0°; (b) 45° and (c) 90°



6 Results and discussion

Two knees with mild and severe OA had been used to demonstrate dynamic visualisation and measurement of cartilage morphology. From Figure 15 showing their AKJM with the cartilage surfaces coloured in purple, the lateral tibiofemoral compartments of both knees on the left are seen to have similar cartilage cover, whereas the medial tibiofemoral compartments of both knees on the right are seen to be significantly different with the severe OA knee seen to have some regions on femur and tibia without cartilage cover leaving bone exposed.

Figure 15 AKJM models: (a) mild OA and (b) severe OA



Applying the proposed method presented in Section 5 to estimate tibial cartilage thickness of both mild and severe OA knees, Figure 16 shows the cartilage coverage on the tibial plateau along its middle elevation profile, computed based on measurement points equally spaced at 0.5 mm

starting from LEP. For the bimodal cartilage thickness profiles shown in Figure 16, the left and right cartilage profiles correspond to the lateral and medial cartilage coverage of the tibial plateau, respectively. Comparing the mild and severe OA knees based on their corresponding left and right cartilage profiles, it is apparent that the mild OA knee has wider cartilage cover than the severe OA knee for both sides, with 16.5 mm against 14.0 mm for the lateral side and 13.5 mm against 7.5 mm for the medial side. Most significantly, the medial tibial cartilage coverage of the severe OA knee is seen to be not only narrower but also thinner compared with the lateral tibial cartilage coverage. While the average tibial cartilage thickness is 3.22 ± 0.05 mm (mean \pm standard deviation) for the mild OA knee, the average tibial cartilage thickness is 2.22 ± 0.11 mm for the severe OA knee.

Applying the proposed method to the same measurement points to estimate the dynamic tibiofemoral cartilage thickness of both mild and severe OA knees, Figure 17 shows the results by using two heatmaps for comparative visualisation, where the X-axis denotes the knee joint angle from 0° to 90° at 1° resolution, the Y-axis denotes the measurement points with respect to LEP at 0.5 mm resolution, with high cartilage thickness denoted by dark red and no cartilage denoted by dark blue. With two horizontal colour varying stripes separated by dark blue in each heatmap, the top and bottom colour stripes reveal the characteristics of the joint angle-based cartilage coverage on the lateral and medial sides, respectively. While the width of each stripe can be used to assess joint angle-based cartilage loss, the colour variation along each stripe can be used to assess joint angle-based cartilage wear pattern.

Figure 16 Tibial cartilage profile: (a) mild OA and (b) severe OA

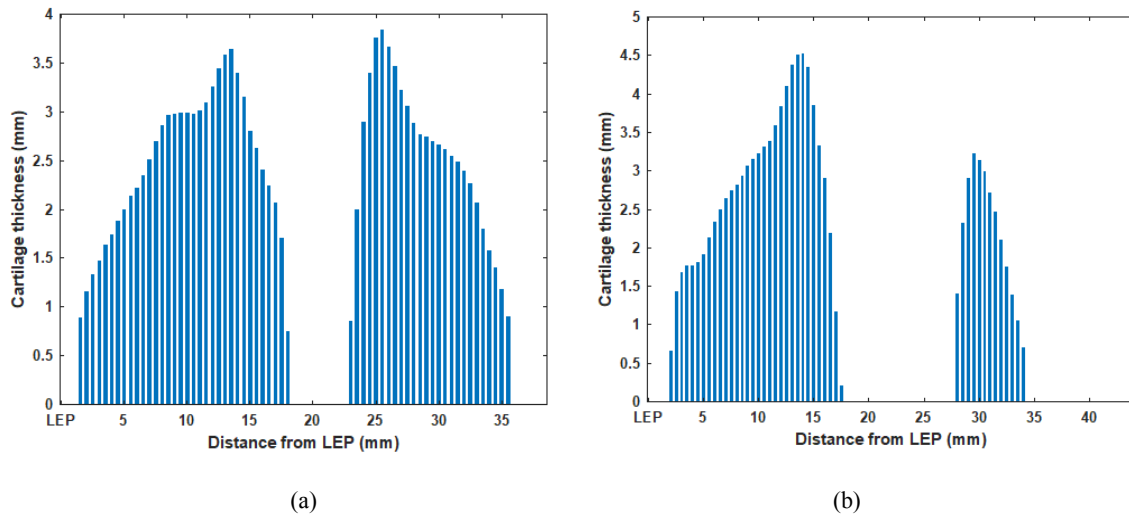
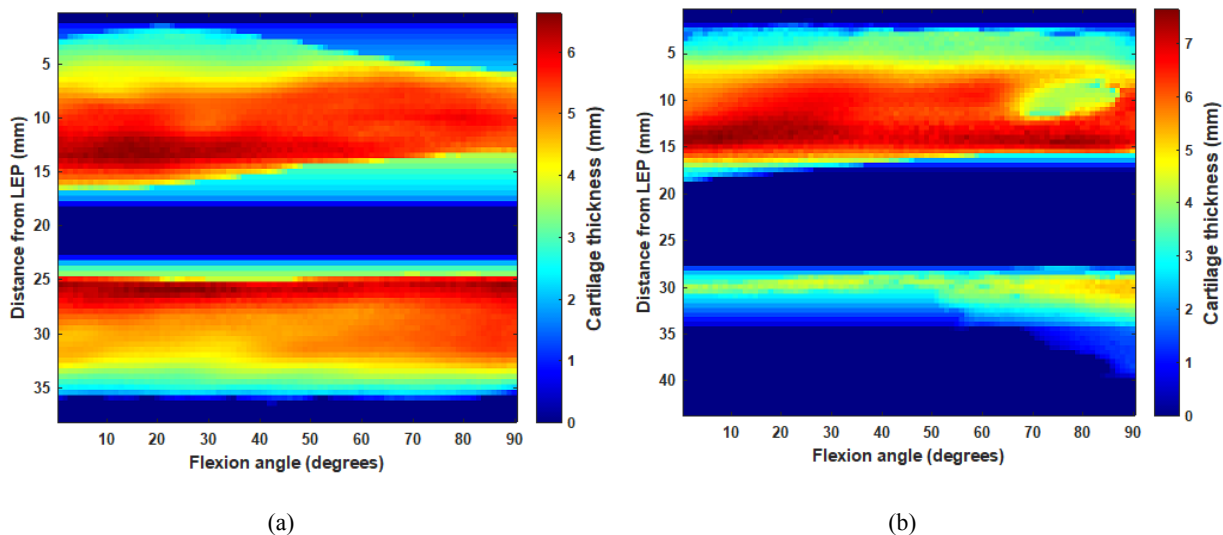


Figure 17 Dynamic tibiofemoral cartilage profile: (a) mild OA and (b) severe OA

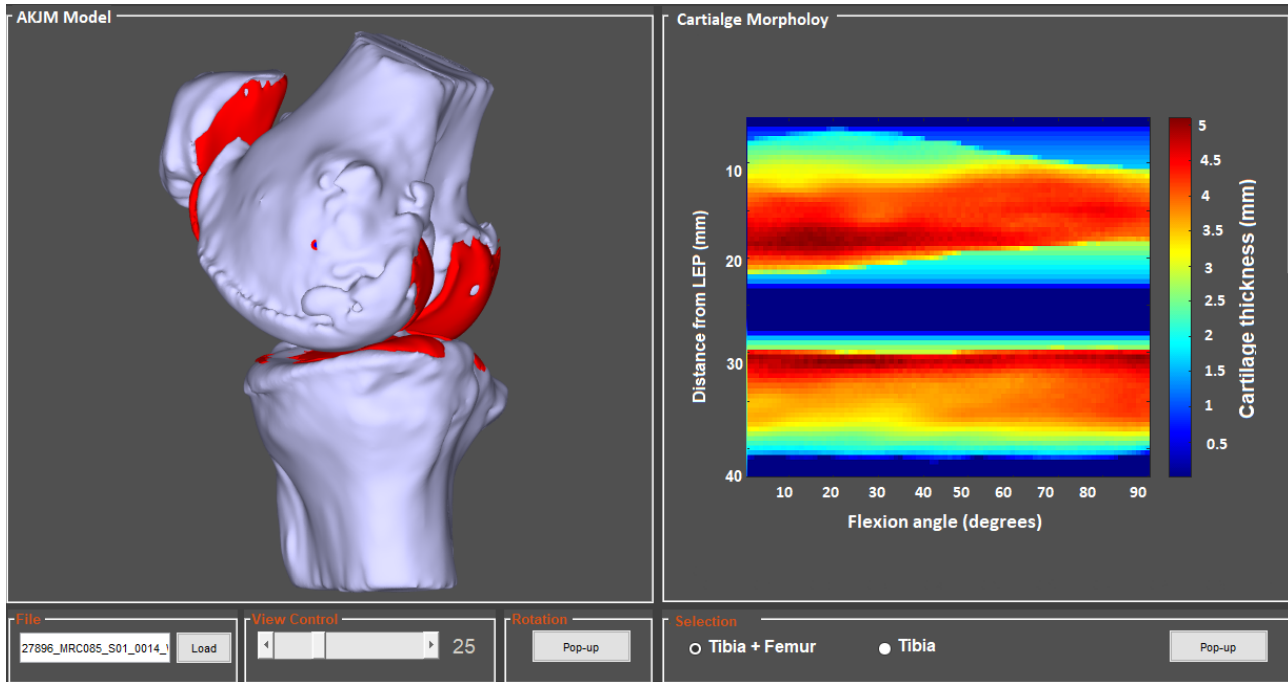


From Figure 17, the differences between the mild and severe OA knees are particularly significant on the medial side of the tibiofemoral joint. While the bottom colour stripe width of the mild OA knee is seen to be wide and relatively constant throughout the whole angular range, the bottom colour stripe of the severe OA is seen to be very narrow and angle-dependent, indicating not only significant cartilage loss, but also more cartilage loss towards 0° joint angle. Furthermore, the colour variation along the bottom stripe reveal a cartilage wear pattern with the cartilage thickness tending to be thinner as joint angle decreases, with this phenomenon being more apparent in the severe OA knee than the mild OA knee.

All of the cartilage morphology characteristics observed from Figures 16 and 17 are consistent with the physical phenomena. While more cartilage loss on the medial tibiofemoral side could be explained by higher load on the medial tibiofemoral joint due to the body's centre of mass being medial to the knee, more cartilage wear around the

knee angle of 0° could be explained by the constant need to withstand the full body weight for standing.

To investigate and demonstrate the potential of the proposed bone-based kinematic approach for dynamic knee joint assessment, an interactive visual tool was implemented using Matlab. A screenshot of the interactive visual tool in operation is shown in Figure 18, where it is seen to consist of two main display windows. For the left display window on the screen, it is used for visualisation of knee joint articulation generated based on the extracted knee kinematic. While the knee flexion angle can be controlled by the sliding bar below, the movement of the knee joints can be viewed from different angles by clicking the Pop-up button. For the right display window on the screen, it is used for visualisation and measurement of the joint angle-based tibiofemoral cartilage thickness morphology. Through the visual tool, comprehensive and meaningful assessment of dynamic knee joints can be performed by cross-checking of knee articulation and corresponding cartilage morphology.

Figure 18 Visual tool for dynamic knee joint assessment

7 Conclusions

Through a novel development of bone-based knee kinematics, this paper presents dynamic visualisation and measurement of knee cartilage morphology as a new clinical tool for qualitative and quantitative assessment of knee joints. From the perspective of implementation requirements, the proposed approach is shown to have a significant advantage of practical simplicity, because anatomy-based emulation of knee joint articulation is derived from simple motion capture of an artificial anatomical knee model. From the perspective of clinical potential, the presented visualisation tool is shown to provide significantly better qualitative and quantitative information for a more comprehensive knee joint diagnosis in a time-effective way. In particular, the availability of coupled tibiofemoral and patellofemoral articulations in 3D offers the possibility of qualitative assessment of whole knee in an intuitive and meaningful manner through joint angle-based interrogation, and the example of the differences between mild and severe OA knees in their dynamic tibiofemoral cartilage thickness demonstrates the possibility of quantitative assessment of articular cartilages in a more comprehensive manner by including additional joint angle-based measurements of contact area, local volume and surface profile.

Future work will focus on increasing the clinical potential. For the proposed bone-based knee kinematics, one aspect for further development is to extend anatomy-based emulation of knee joint articulation from pure extension/flexion movements to more complex movements involving adduction/abduction and internal/external rotations, and this can be achieved by using more than one camera for motion capture of position and orientation markers placed on either an artificial anatomical knee model or a human knee joint, thereby enabling dynamic knee joint assessment to be performed in high degrees of

freedom. For the proposed visualisation tool, a particular focus will be on development of a comprehensive suite of functions for quantitative measurement of dynamic cartilage morphology of both tibiofemoral and patellofemoral joints, thereby enabling it to serve as a new clinical tool to support comprehensive knee joint assessment.

References

- Balamoody, S., Williams, T.G., Waterton, J.C., Bowes, M., Hodgson, R., Taylor, C.J. and Hutchinson, C.E. (2010) 'Comparison of 3T MR scanners in regional cartilage-thickness analysis in osteoarthritis: a cross-sectional multicenter, multivendor study', *Arthritis Research and Therapy*, Vol. 12, No. 5, pp.1–9.
- Chen, H-C., Wu, C-H., Wang, C-K., Lin, C-J. and Sun, Y-N. (2013) 'A Joint-constraint model-based system for reconstructing total knee motion', *IEEE Transactions on Biomedical Engineering*, Vol. 61, No. 1, pp.171–181.
- D'Lima, D.D., Fregly, B.J., Patil, S., Steklov, N. and Colwell, C.W. (2012) 'Knee joint forces: Prediction, measurement, and significance', *Proceedings of the Institution of Mechanical Engineers, Part H*, Vol. 226, No. 2, pp.95–102.
- Eckstein, F., Cicuttini, F., Raynauld, J.P., Waterton and Peterfy, C. (2006) 'Magnetic resonance imaging (MRI) of articular cartilage in knee osteoarthritis (OA): Morphological assessment', *Osteoarthritis Cartilage*, Vol. 14, No. Suppl. A, pp.A46–A75.
- Gahunia, H.K., Gross, A.E., Pritzker, K.P.H., Babyn, P.S. and Murnaghan L. (2020) *Articular Cartilage of the Knee*, Springer.
- Grochow, K., Martin, S.L., Hertzmann, A. and Popović, Z. (2004) 'Style-based inverse kinematics', *ACM Transactions on Graphics*, Vol. 23, No. 3, pp.522–531.
- Hamai, S., Dunbar, N.J., Moro-oka, T-A., Miura, H., Iwamoto, Y. and Banks, S.A. (2013) 'Physiological sagittal plane patellar kinematics during dynamic deep knee flexion', *International Orthopaedics*, Vol. 37, No. 8, pp.1477–1482.

Dynamic visualisation and measurement of cartilage morphology

- Kainz, H., Modenese, L., Lloyd, D.G., Maine, S., Walsh, H.P.J. and Carty, C.P. (2016) 'Joint kinematic calculation based on clinical direct kinematic versus inverse kinematic gait models', *Journal of Biomechanics*, Vol. 49, No. 9, pp.1658–1669.
- Kedgley, A.E., McWalter, E.J. and Wilson, D.R. (2015) 'The effect of coordinate system variation on in vivo patellofemoral kinematic measures', *Knee*, Vol. 22, No. 2, pp.88–94.
- Kucuk, S. and Bingul, Z. (2006) *Robot Kinematics: Forward and Inverse Kinematics*, INTECH Open Access Publisher.
- Lloyd, D.G. and Besier, T.F. (2003) 'An EMG-driven musculoskeletal model to estimate muscle forces and knee joint moments in vivo', *Journal of Biomechanics*, Vol. 36, No. 6, pp.765–776.
- Meister, B.R., Michael, S.P., Moyer, R.A., Kelly, J.D. and Schneck, C.D. (2000) 'Anatomy and kinematics of the lateral collateral ligament of the knee', *The American Journal of Sports Medicine*, Vol. 28, No. 6, pp.869–878.
- NICE (2014) *Osteoarthritis: Care and Management*, National Institute for Health and Care Excellence Clinical Guideline. Available online at: <https://www.nice.org.uk/guidance/cg177>
- Reinbolt, J.A., Schutte, J.F., Fregly, B.J., Koh, B.I., Haftka, R.T., George, A.D. and Mitchell, K.H. (2005) 'Determination of patient-specific multi-joint kinematic models through two-level optimization', *Journal of Biomechanics*, Vol. 38, No. 3, pp.621–626.
- Shark, L-K., Huang, K., Quan, W., Waterton, J.C., Bowes, M.A. and Goodacre, J. (2016) 'Acoustic emission sonification and magnetic resonance imaging-based kinematics for exploratory analysis of knee joints', *Proceedings of the IEEE International Conference on Bioinformatics and Biomedicine (BIBM)*, Shenzhen, China, pp.1016–1022.
- Song, S.Y., Pang, C.H., Kim, C.H., Kim, J., Choi, M.L. and Seo, Y.J. (2015) 'Length change behavior of virtual medial patellofemoral ligament fibers during in vivo knee flexion', *American Journal of Sports Medicine*, Vol. 43, No. 5, pp.1165–1171.
- Sowers, M.F., Hayes, C., Jamadar, D., Capul, D., Lachance, L., Jannausch, M. and Welch, G. (2003) 'Magnetic resonance detected subchondral bone marrow and cartilage defect characteristics associated with pain and X-ray-defined knee osteoarthritis', *Osteoarthritis Cartilage*, Vol. 11, No. 6, pp.387–393.
- Spain, L., Rajoub, B., Schlüter, D.K., Waterton, J., Bowes, M., Shark, L-K., Diggle, P. and Goodacre, J. (2015) 'Biomarkers for knee osteoarthritis: new technologies, new paradigms', *The International Journal of Clinical Rheumatology*, Vol. 10, No. 4, pp.287–297.
- Tischer, T., Geier, A., Lenz, R., Woernle, C. and Bader, R. (2016) 'Impact of the patella height on the strain pattern of the medial patellofemoral ligament after reconstruction: a computer model-based study', *Knee Surgery, Sports Traumatology, Arthroscopy*, Vol. 24, No. 207, pp.1–11.
- Wang, J., Zhu, Q., Wang, W., and Zhao, L. (2014) 'Straight line extraction algorithm by Hough transform combining edge grouping', *Journal of Remote Sensing*, Vol. 18, pp.384–389.
- Wang, Z., Quan, W. and Shark, L-K. (2022) 'Development of bone-based kinematics from magnetic resonance imaging for immersive assessment of knee joint', *Proceedings of the 5th International Conference on Image and Graphics Processing*, Beijing, China, pp.174–182.
- Wick, M.C., Kastlunger, M. and Weiss, R.J. (2014) 'Clinical imaging assessments of knee osteoarthritis in the elderly: a mini-review', *Gerontology*, Vol. 60, No. 5, pp.386–394.